SPANDIDOS PUBLICATIONS

Fourier transform infrared spectromicroscopy and hierarchical cluster analysis of human meningiomas

KAISER ALI[1], YANJIE LU[2], COLLEEN CHRISTENSEN[3], TIM MAY[3], CRAIG HYETT[3], ROBERT GRIEBEL[4], DARYL FOURNEY[4], KOTOO MEGURO[4], LOTHAR RESCH[5] and RAJENDRA K. SHARMA[2,5]

[1]Saskatoon Cancer Centre, Cancer Research Unit, Saskatchewan Cancer Agency, and University of Saskatchewan, 20 Campus Drive, Saskatoon S7N 4H4; [2]Cancer Research Unit, Saskatchewan Cancer Agency, 20 Campus Drive, Saskatoon S7N 0X4; [3]Canadian Light Source, University of Saskatchewan Campus, 101 Perimeter Road, Saskatoon S7N 0X4; Departments of [4]Neurosurgery, [5]Pathology, University of Saskatchewan, Royal University Hospital, 103 Hospital Drive, Saskatoon S7N 0W8, Canada

Received August 28, 2007; Accepted October 8, 2007

Abstract. Limitations of conventional light microscopy in pathological diagnosis of brain tumors include subjective bias in interpretation and discordance of nomenclature. A study using mid-infrared (IR) spectromicroscopy was undertaken to determine whether meningiomas, a group of brain tumors prone to recurrence, could be identified by the unique spectral 'fingerprints' of their chemical composition. Paired, thin (5-μm) cryosections of snap-frozen human meningioma tumor samples removed at elective surgery were mounted on glass (hematoxylin and eosin-stained tissue section) and infrared (unstained tissue section) reflectance slides, respectively. Concordance of the tumor-bearing areas identified in the stained section by a pathologist with the unstained IR tissue section was ensured using a novel digital grid and tumor-mapping system developed in our laboratory. Compared with the normal control, tumor samples from four meningioma patients revealed a marked decrease in bands associated with unsaturated fatty acids, particularly in the bands at 3010, 2920, 2850, and 1735 cm^{-1}. Spectral datasets were subjected to hierarchical cluster analyses (HCA) using Ward's algorithm for comparison and grouping of similar data groups, and were converted into color-coded digital maps for matching spectra with their respective clusters. False color images of 5 and 6 clusters obtained by HCA identified dominant clusters corresponding to tumor tissue. Corroboration of these findings in a larger number of meningiomas may allow for more precise identification of these and other types of brain tumors.

Correspondence to: Dr Kaiser Ali, University of Saskatchewan, 20 Campus Drive, Saskatoon S7N 4H4, Canada
E-mail: kaiser@scf.sk.ca

Key words: mid-IR spectromicroscopy, meningiomas, hierarchical cluster analysis

Introduction

Brain tumors are the most common type of malignant solid tumor in childhood, and rank 15th in frequency amongst all cancers in adults (1). Curative management of human brain tumors requires accuracy of histological diagnosis and grading, acquiring tumor-free margins by surgical excision, and demands radiation therapy conforming to the boundaries of tumor-bearing areas detected by magnetic resonance and computerized tomography imaging studies.

Currently, for purposes of diagnostic classification including that of the World Health Organization (2), brain tumor sections stained with hematoxylin and eosin (H&E) as well as an array of immunohistochemical neuronal marker proteins, are scrutinized and categorized by means of light microscopy. These conventional techniques used for classification, however, are prone to subjective interpretation, as well as to the limitations of light microscopy. The reported recognition of brain tumors containing multiple phenotypes (3), as well as newly evolving variants (4), are compelling reasons for developing more refined and accurate diagnostic tools to meet these emerging challenges. Over the past two decades a newer investigational technique, vibrational spectroscopy, is being increasingly applied to provide more accurate differentiation between normal brain tissue (5) and brain tumors (6), as well as for identifying prognostic indicators (7).

Meningiomas comprise a group of brain tumors with significant risks of recurrence and unpredictable outcomes (8). We investigated, by means of mid-infrared spectromicroscopy, a group of meningiomas in order to determine their spectral signatures, and to more accurately differentiate tumor tissue from normal control.

Materials and methods

Acquisition and preparation of samples. With prior informed consent, brain tumor samples were obtained at elective surgery from four patients with meningiomas and are summarised in Table I. A control sample was derived from normal brain

Table I. Clinical summary of meningioma patients.

Case no.	Age in years/sex	Tumor grade (W.H.O. classification)	Intracranial location
1	69/female	Grade 1	Posterior fossa
2	50/male	Grade 1	Right frontal lobe
3	73/female	Grade 1	Right sphenoid
4	73/female	Grade 1	Right occipital

tissue identified at the periphery of resected margins of a meningioma. After dispatching the first tissue aliquot for diagnostic studies, a second specimen was snap-frozen in liquid nitrogen within 30 min of removal, then stored in a freezer at -80˚C in preparation for H&E staining, mid-infrared (IR) spectroscopy and, as part of a correlative study, for N-myristoyltransferase assays (9). Paired tumor tissue sections (5-μm) were cut in a cryostat at -20˚C (Leica CM 1900-3-1, Germany). The first section was placed on a glass slide for H&E staining, and the section immediately following was transferred onto a slide with an IR-reflective coating (Kevley Technologies, Chesterland, OH) for mid-IR spectromicroscopy studies. Concordance of tumor-bearing areas was achieved by means of a novel technique developed in our laboratory. This technique required superimposing a digital tractile grid over paired H&E and IR tissue section images, demarcation of tumor-bearing areas within the tissue section, and then transferring matching grid coordinates onto the overview image generated by the spectromicroscope in preparation for mid-IR spectroscopy (Ali *et al*, unpublished data) (Fig. 1).

Mid-IR microscopy data collection. A 5-μm tumor section on the IR reflectance slide was raster scanned using Fourier transform infrared (FTIR) spectromicroscopy at the Canadian Light Source Synchrotron facility located on campus at the University of Saskatchewan. Spectromicroscopy was performed using an IFS 66v/S FTIR spectrometer with a globar light source attached to a Hyperion IR microscope (Bruker Optics Inc., Billercia, MA) with a x15 Cassegrain objective and a single-channel MCT detector. Raster scans were obtained in the mid-infrared range of 4000-900 cm^{-1} using a 50 μm x 50 μm aperture, a 25-μm step size, 32 scans per step, and a resolution of 4 cm^{-1}. Stage control, data collection and processing were conducted using OPUS software and analysed using CytoSpec (CytoSpec Inc., Boston, MA) a software tool designed for FTIR image analysis. Visible images were obtained using a charged-couple device (CCD) camera, which was linked to the infrared images.

Data processing and multivariate analyses. The spectral datasets were loaded into the analysis package, the second derivative was calculated, and the derivative datasets were then normalized to reduce any sampling artifacts. A statistical analysis of this data was performed using a hierarchical clustering algorithm (Ward's algorithm) which compares the individual elements of the dataset and classifies them into groups (clusters) based on their similarity with other elements of the dataset. This classification process, known as hierarchical cluster analysis (HCA), can then be used to look at the entire dataset as a color-coded map, matching spectra with their respective clusters. The average spectrum can also be calculated for each cluster and compared across samples.

Results

The average spectra shown in Fig. 2a-d compare two different brain tissue samples, control and tumor, each from a different patient. The tumor tissue shown in this figure is from case no. 2, Table I. The source of the control sample was normal brain tissue obtained from outlying resected margins of a brain tumor patient; a pathologist confirmed that this sample was free of tumor. The study sample was derived from histologically confirmed tumor tissue resected from another patient.

Fig. 2a and b shows that one of the clusters from within the tumor sample is broadly similar to the control spectra, with some dissimilarities as indicated in the accompanying legend. On the other hand, Fig. 2c and d contrast three similar clusters (one average control spectrum and two average malignant tumor-derived clusters) showing several important differences. The first, most striking difference occurs in the bands associated with lipids, particularly unsaturated fatty acids, demonstrating a marked decrease in all the clusters associated with tumor tissue. In particular, the bands at 3010, 2920, 2850, and 1735 cm^{-1} are all weaker than in the control spectra. More subtle differences are visible in the region between 1800-900 cm^{-1}, particularly among the protein bands. The amide I band of the control tissue shows a large proportion of undifferentiated proteins and a small contribution of α-helical proteins at 1655 cm^{-1}. The tumor tissue samples tend more towards undifferentiated proteins; however, some of the clusters show an increased ß-sheet band at 1631 cm^{-1}. The amide II region of the tumor samples also shows a potentially significant 4-cm^{-1} shift relative to the control spectra, from 1548 to 1544 cm^{-1}. Finally, a band generally associated with the amino acid tyrosine at 1515 cm^{-1} was generally more pronounced in the tumor samples than in the control samples.

Fig. 3 displays the results of the HCA calculations. Fig. 3a is a dendrogram plot demonstrating the separation of clusters, and their hierarchy, developed by the algorithm. At the top, all spectra are members of one or two very distinct clusters; however, as the number of clusters is increased, the number of spectra in each cluster is reduced. More importantly, the separation of individual clusters, which represents differences in a given cluster from its neighbors, becomes increasingly critical. At the bottom of the dendrogram plot,

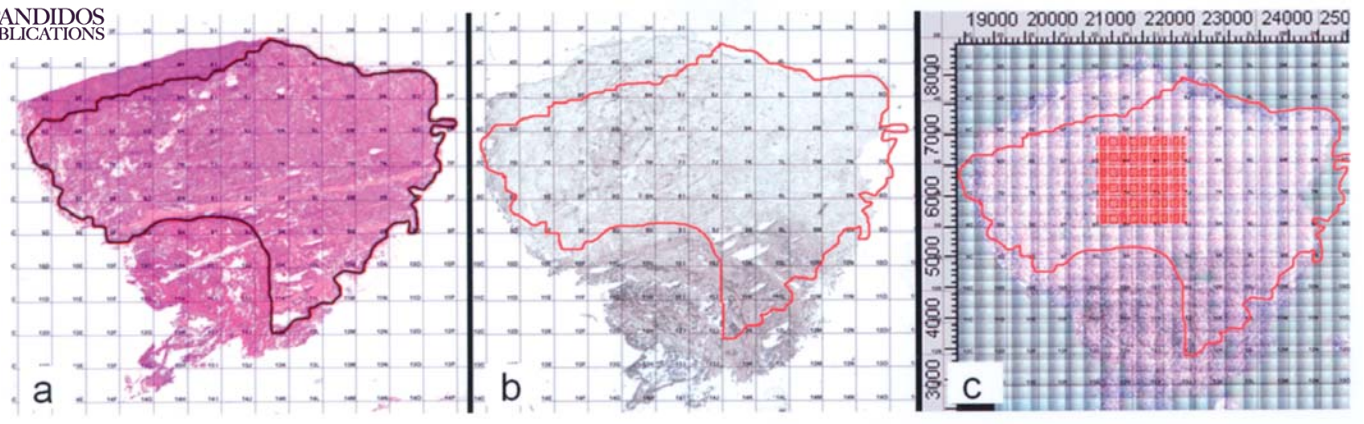

Figure 1. (a) Equisized H&E-stained tissue section with concordant grid and tumor-bearing area within digital boundaries (outlined in black). (b) Equisized paired IR unstained tissue section showing tumor-bearing area (within red boundaries) with concordant grid and overlaid digital boundary map transferred from Fig. 3a. (c) Equisized spectromicroscopy overview image of tissue section with raster map (red square) outlined within tumor-bearing area (within red boundaries), in preparation for mid-IR spectroscopy (note matched grid coordinates in all images).

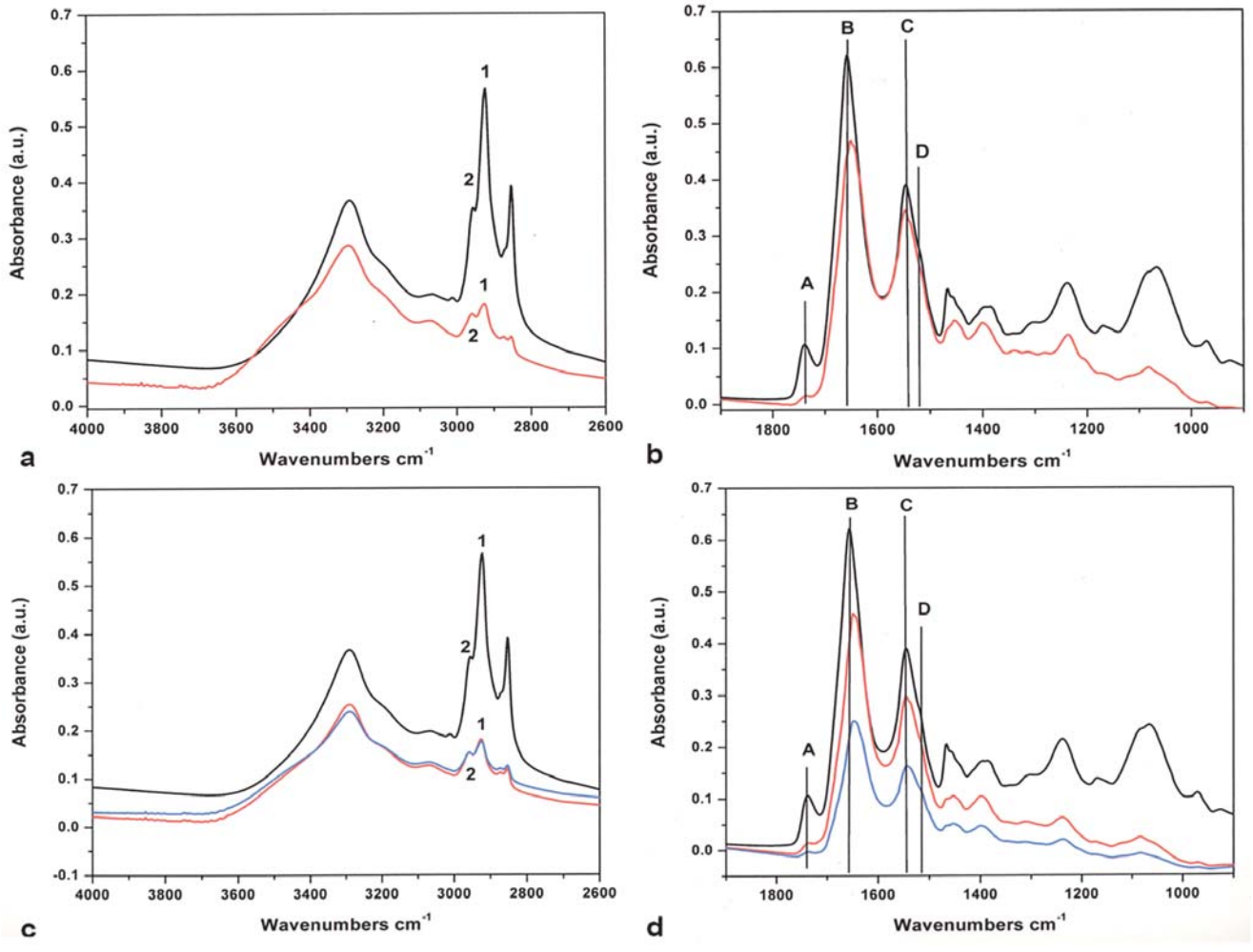

Figure 2. (a) The average control spectrum (black) and an average cluster from the cancer tissue (red) which is found to be broadly similar. Despite the spectral similarities the relative CH_2/CH_3 stretching intensities are very different (labeled 1 and 2 respectively). (b) The average control spectrum (black) and an average cluster from the cancer tissue (red) which is found to be broadly similar: A (1735 cm^{-1}) shows a large decrease in lipid concentration (1735 cm^{-1}), B (1655 cm-1) shows the amide I peak is largely unchanged from the control sample, C (1548 cm^{-1}) shows that the amide II is largely unchanged from the control sample, and D (1515 cm^{-1}) is very similar to the control sample. (c) The average control spectrum (black) and two average clusters from the cancer tissue (red and blue) which indicate marked differences with the control sample, particularly in the relative CH_2/CH_3 stretching intensities (labeled 1 and 2 respectively). (d) The average control spectrum (black) and two average clusters from the cancer tissue (red and blue) which illustrate a marked difference with the control sample: A (1735 cm^{-1}) shows a large decrease in lipid concentration (1735 cm^{-1}), B (1655 cm^{-1}) shows that the amide I peak shifts towards 1631 cm^{-1}, C (1548 cm^{-1}) shows that the amide II shifts to 1544 cm^{-1}, and D (shoulder at 1515 cm^{-1}) has increased intensity relative to the control sample.

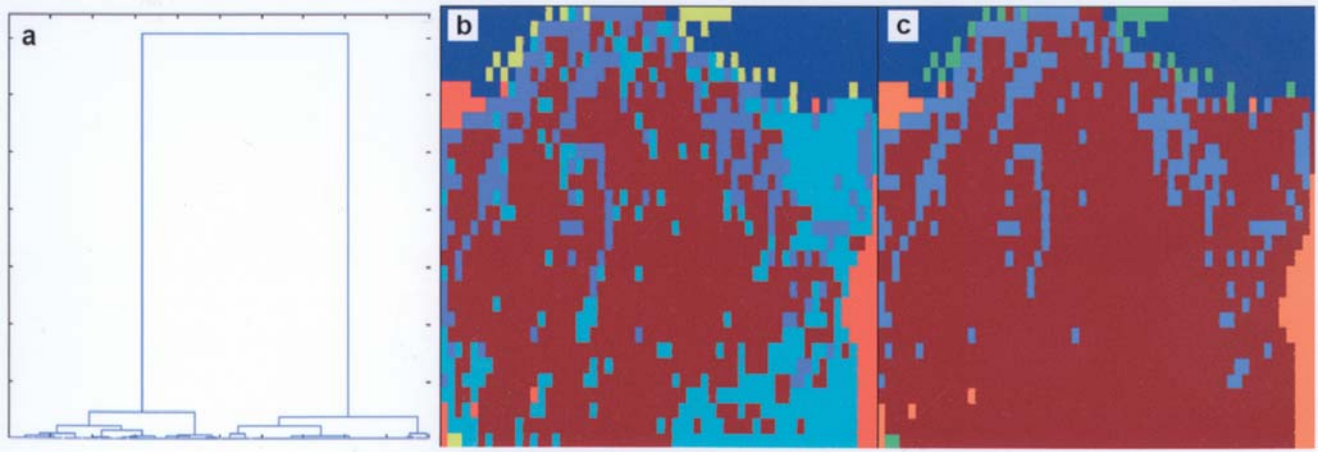

Figure 3. (a) Dendrogram plot derived from the HCA method demonstrating hierarchy of separated clusters derived from tumor tissue. (b) HCA false color image of 6 clusters, displaying predominance of tumor tissue as the brown cluster. (c) HCA false color image of 5 clusters, also displaying predominance of tumor tissue as the brown cluster (darker blue clusters in both this and the preceding image correspond to those closely resembling control spectra from Fig. 2).

the individual spectra each make up their own cluster, and it is possible to see just how well separated and different these are.

By color coding these clusters and assigning each pixel a color, the false color images shown in Fig. 3b and c can be generated. These false color images show the spatial distribution of the clusters in the image, where b displays 6 clusters and c displays 5 clusters. The images in Fig. 3b and c demonstrate the spatial distribution of the various clusters identified by the HCA algorithm. In both cases, the algorithm assigned one cluster to the pixels off the edge of the sample, a second cluster was assigned to the edge of the sample, and two or three clusters were assigned to the sample. In both images it is obvious that the brown cluster dominates, and this cluster corresponds to one of the average spectra of brain tumor tissue identified in Fig. 2, as does the pale blue cluster in Fig. 3b. On the other hand, the darker blue cluster in both images appears to correspond to clusters that closely resemble control spectra from Fig. 2. These cluster images demonstrate the ability of a spectromicroscopic technique to highlight differences not readily detected by the naked eye.

Discussion

Mid-infrared spectromicroscopy is a relatively new tool that can contribute to more accurate and precise diagnoses and classifications of malignant tumors in the brain and other organs. By capturing the pattern of vibrational bonds and the spatial distribution of molecular arrangements within biological tissues, it creates and displays characteristic spectral patterns or 'molecular fingerprints' that reveal the biological structure unique to normal tissues and their malignant counterparts. This information, combined with conventional diagnosis and grading of tumors, will allow for planning of more precise and individualized treatment for each patient, with the potential for improving cure rates and long-term survival in cancer patients.

The results to date indicate the presence of a unique signature that could help identify tumor tissue. The marked diminution of the bands associated with the lipids combined with subtle changes in the main protein bands seems to be an indicator that a sample tissue is derived from a tumor. This fingerprint was similar for all of the different samples studied to date, and it may be possible to refine this spectral fingerprint to detect a specific tumor class. This text refers to results obtained from case no. 2 (Table I); comparable results were found in three other patients with meningiomas (Table I). One of the strengths of this study was that, in spite of the small number of samples, all four patients had the same type and grade of tumor confirmed by a pathologist. This avoided the potential problem arising from the interpretation of disparate degrees of anaplasia within the same histological tumor type.

The application of HCA as a statistical technique in tumor detection is applicable not just to brain tumors, but to all malignant tumors. Potential research applications of HCA include, among others, determining biochemical differences between normal and tumor cells as a means of detecting the etiology of malignant tumors. It also has potential practical application as an intraoperative diagnostic tool for determining whether the neurosurgeon has achieved removal of microscopic residual tumor cells in biopsy samples taken from the margins of resected tumors.

The use of HCA for image analysis has some limitations that must be overcome before it can be used outside of a research setting. Most notably, these techniques are statistical in nature, and their fidelity depends on the quality of the data provided for analyses. In order to ensure reliable results from the algorithms, the spectra must first have a high signal-to-noise ratio. In addition, the number of samples is very important, not only for overcoming inherent heterogeneity of biological samples, but also for separating the individual spectra into clusters that have anatomical and biochemical relevance. We therefore plan to generate incremental data by expanding our study to include a larger number of human meningioma samples.

Conventional IR spectromicroscopy examination of biological tissues has limitations (10-12) including an insufficient spatial resolution of only ~20-25 μm. These problems are overcome by synchrotron IR light by virtue of

iess, which is 100-1000 times greater than that from ional source (13). Individual biological cells range from 5-30 μm in diameter, too small for probing by conventional IR sources. The much greater brightness of synchrotron light, however, permits intracellular imaging of molecular chemical structure and, compared to globar IR light sources, may provide greater spectroscopic detail that could serve as a more refined diagnostic tool for a spectrum of malignant brain tumors, both in terms of differentiating tumor types as well as assessing the degree of anaplasia. Future studies will include performing mid-IR experiments on human meningiomas using synchrotron-derived mid-IR light, and we plan to compare these results with those obtained from this study using globar-source mid-IR light in order to determine whether the former will provide improved diagnostic spectral patterns.

The potential usefulness of FTIR lies in the fact that once specific tumor spectral patterns can be identified and corroborated, it has the potential to eliminate subjective bias that is inherent in conventional diagnostic techniques requiring a pathologist's interpretation of visual light microscopy findings in stained tissue sections. Limitations of FTIR at the present time include the fact that FTIR spectroscopy can only be performed on dead tumor tissue removed from human patients. To be truly useful as a diagnostic tool, it should allow study of fresh tumor specimens in order to provide accurate information to guide the neurosurgeon in the operating room. It must also have relevance for the radiation oncologist, whenever radiation therapy is integrated into multimodality treatment plans.

These results are a first step in the use of infrared spectromicroscopy as a means of identifying meningiomas, a particular histological group of human brain tumors. The subtle spectral fingerprints of this tumor type have been identified with the aid of hierarchical clustering analysis. Corroboration of these findings in a larger number of meningiomas may allow for more precise identification of particular classes or subtypes of tumors, and for grading degrees of anaplasia within tumors. As well, they may reveal spectral fingerprints distinguishing new tumors arising *de novo* from those that recur, the latter situation being a frequent complication in cases of meningiomas.

Acknowledgements

The research described in this paper was performed at the Canadian Light Source, which is supported by NSERC, NRC, CIHR, and the University of Saskatchewan. We thank Dr Michael Jackson, National Research Council, Winnipeg, for his unstinting support and expert advice, Shannon Klassen, A.R.T., Department of Pathology, Saskatoon City Hospital for preparation of the cryostat tissue sections, and Stefanie Drummond, Provincial Pediatric Oncology Program, Saskatoon Cancer Centre, for secretarial assistance. This study was funded in part by the Saskatchewan Synchrotron Institute and College of Medicine, University of Saskatchewan, and by the Canadian Institute of Health Research Grant MOP-36484 to Dr Rajendra K. Sharma.

References

1. Canadian Cancer Society/National Cancer Institute of Canada: Canadian Cancer Statistics, Toronto, Canada 2006. ISSN 0835-2976, April 2006.
2. Gonzales M: The 2000 World Health Organization classification of tumors of the nervous system. J Clin Neurosci 8: 1-3, 2001.
3. Jay V, Edwards V, Halliday W, Rutka J and Lau R: Polyphenotypic tumors in the central nervous system: problems in nosology and classification. Pediatr Pathol Lab Med 17: 369-389, 1997.
4. Cenacchi G and Giangaspero F: Emerging tumor entities and variants of CNS neoplasms. J Neuropathol Exp Neurol 63: 185-192, 2004.
5. Jackson M, Choo LP, Watson PH, Halliday WC and Mantsch HH: Beware of connective tissue proteins: assignment and implications of collagen absorptions in infrared spectra of human tissues. Biochim Biophys Acta 1270: 1-6, 1995.
6. Krafft C, Thümmler K, Sobottka SB, Schackert G and Salzer R: Classification of malignant gliomas by infrared spectroscopy and linear discriminant analysis. Biopolymers 82: 301-305, 2006.
7. Asgari S, Röhrborn HJ, Engelhorn T and Stolke D: Intraoperative characterization of gliomas by near-infrared spectroscopy: possible association with prognosis. Acta Neurochir 145: 453-460, 2003.
8. Drummond KJ, Zhu JJ and Black P: Meningiomas: Updating basic science, management, and outcome. Neurologist 10: 113-130, 2004.
9. Lu YJ, Selvakumar P, Ali K, Shrivastav A, Bajaj G, Resch L, Griebel R, Fourney D, Meguro K and Sharma RK: Expression of N-myristoyltransferase in human brain tumors. J Neurochem Res 30: 9-13, 2005.
10. Carr GL: Resolution limits for infrared microspectroscopy explored with synchrotron radiation. Rev Sci Instr 72: 1613-1619, 2001.
11. Xie AH, He Q, Miller L, Sclavi B and Chance MR: Low frequency vibrations of amino acid homopolymers observed by synchrotron far-IR absorption spectroscopy: Excited state effects dominate the temperature dependence of the spectra. Biopolymers 49: 591-603, 1999.
12. Williams GP: The initial scientific program at the NSLS infrared beamline. Nuclear Instruments & Methods in Physics Research Section A-Accelerators Spectrometers Detectors and Associated Equipment 291: 8-12, 1990.
13. Duncan WD and Williams GP: Infrared synchrotron radiation from electron storage-rings. Appl Opt 22: 2914-2923, 1983.